MINERALOGY OF HALLOYSITES AND THEIR INTERACTION WITH PORPHYRINE

#VLASTA VAŠUTOVÁ, PETR BEZDIČKA*, KAMIL LANG*, DAVID HRADIL*

Charles University in Prague, Faculty of Science, Albertov 6, 128 43 Prague, Czech Republic
**Institute of Inorganic Chemistry of the AS CR, v.v.i., Husinec-Řež 1001, 250 68 Řež, Czech Republic*

#E-mail: vasutovavlasta@seznam.cz

Submitted March 6, 2013; accepted June 16, 2013

Keywords: Organoclays, Mineralogy, Halloysite, Porphyrine, CEC

Samples representing two modifications of halloysites, dehydrated (7 Å) and hydrated (10 Å) forms, respectively, were examined with the aim to select suitable candidates for to be used as carriers of porphyrine photoactive molecules. The samples were analysed by powder X-ray diffraction (pXRD), infrared spectroscopy (FT-IR), and high resolution transmission electron microscopy (HRTEM). Chemical composition was also determined. For the determination of cationic exchange capacity (CEC) the silver thiourea method (AgTU) was used. Silver cations concentrations in the solution before and after the interaction were determined by atomic absorption spectrometry (AAS). By the interaction of two pure hydrated halloysites with porphyrine it was found that porphyrine does not intercalate the interlayer space, but it is adsorbed on the outer surface of halloysite. This interaction changed the colour of clay sample from white to green. The changes were also clearly visible on diffuse reflectance spectra (DRS).

INTRODUCTION

Halloysite is a clay mineral belonging to the group of kaolinite. Chemical formula of fully hydrated halloysite is $Al_2Si_2O_5(OH)_4 \cdot 2H_2O$. Actual width of its interlayer depends on a grade of hydration of halloysite [1]. It occurs in two main modifications - as dehydrated (7 Å) halloysite and hydrated (10 Å) halloysite. The content of water in the interlayer at halloysite 10 Å is about 12.3 wt. % [2]. It dehydrates very fast into the halloysite 7 Å by the sinking humidity and this process is irreversible [3-6]. Halloysites can also be classified according their morphology and ordering of their structure.

Three main morphological types can be found: platy, tubular and spherical halloysites, respectively [7-9]. Transmission electron microscopy (TEM) is the most suitable method for the morphological descriptions of halloysites [2]. Tubular morphology predominates [10, 11].

Admixtures to natural halloysites are very often - other clay minerals, iron oxides, poorly crystalline or amorphous phases can be placed into the halloysite tubes. The increased concentration of iron can be related either with the presence of free oxides (e.g. hematite), or with the partial replacement of Al^{3+} by Fe^{3+} in octahedral sheets of halloysite [5, 8, 9, 11]. The isomorphic substitution of Si^{4+} by Fe^{3+} in tetrahedral position was not ever mentioned [5].

Halloysite is formed predominantly in tropical and subtropical areas by the weathering of igneous rocks or by the hydrothermal alteration, respectively [5, 12-15].

Halloysite is exploited and commercially used in ceramic industry and production of porcelain, similarly to kaolinite [15]. Further it is used as the admixture in pigments, sealing materials, lubricants, pesticides, domestics, groceries and cosmetic products [5]. Particles of halloysite have an unusual tubular morphology becoming a frequent subject of scientific researches in the last century.

These nanotubes can serve as matrices for a sorption of different organic molecules [3, 16-22]. The morphology, hydration properties and sorption and ion-exchange properties of halloysite have influence on its interactions with salts and organic molecules. Frequently the halloysites are used as components of polymers as well [23-26]. Presently a looking for the minerals usable as carriers of photoactive molecules (e.g. porphyrine) starts to be frequent subject of scientific researches [27]. Porphyrine is able to produce singlet oxygen by the interaction with solar radiation and it causes dissociation of other organic compounds. While the single porphyrine is usually removed from organic mixtures very easily, adsorbed on suitable mineral (e.g. clay mineral) becomes very stable. The aim of this study was to characterize halloysites from different economically important deposits cross-over the world and try to interact the most

perspective candidates with porphyrine. The mineralogical composition of all the samples, their particle size and morphology as well as cation exchange capacity and hydration properties has been investigated.

EXPERIMENTAL

Materials

Within this study one commercial sample (supplied by Sigma-Aldrich) and eleven raw halloysites from Slovakia, Turkey, China, New Zealand and U.S.A., respectively, have been characterized (Table 1). For the analytical and experimental purposes samples were divided into two separate portions. One portion was powdered before each measurement (bulk sample) and the other portion of the material was disaggregated in distilled water; a fine clay fraction was then used to prepare an oriented specimen by the slow sedimentation of clay suspension on a glass slide, and drying in air (OP sample) [28]. The ultrasonic treatment was applied to avoid the formation of aggregates. With the aim to distinguish diffraction lines of halloysite and kaolinite some of OP samples were sprayed with fine aerosol of formamide (formamide min. 99 % GC, Sigma - Aldrich) before their measurement.

Cation exchange capacity (CEC)

The cation exchange capacity (CEC) of halloysites was determined by the method described by Dohrmann [29]. This method is based on the interaction of clay minerals with the stock solution of silver - thiourea (AgTU; 7.6 g of thiourea, 1.6690 g of silver nitrate, and 100 ml of 1M solution of ammonium acetate per 1000 ml of the stock solution). It is very suitable for the determination of relatively low values of CEC as expected in the case of halloysites. Within background experiments we have specified more precisely the optimal solid/liquid ratio which should be at least 1:20 to get the maximal availability of the whole surface area for the solution.

At first, all samples were homogenized in an agate mortar and then the appropriate amount of each sample was placed into 80 ml plastic flask and the stock solution of AgTU was added (1 g of sample per 20 ml of AgTU and 0.5 g of sample per 10 ml of AgTU, respectively to keep the solid/liquid ratio at 1:20). These suspensions were then shaked for two hours and centrifuged. The supernatant was then poured off into the volumetric flask containing already 10 or 5 ml of 0.5 M solution of nitric acid, respectively, to avoid the precipitation of Ag^+ ions. The residual samples were then washed twice with distilled water and centrifuged again; the supernatant was added into the volumetric flask too. After the washing all volumetric flasks were filled up with distilled water to the total volume 100 or 50 ml, respectively.

The final values of CEC were calculated from concentration differences of Ag^+ ions in the stock and interacted solutions, respectively, determined by atomic absorption spectrometry (AAS) using the Carl-Zeiss Jena spectrometer (flame - air) with the wavelength of 328.1 nm, width of slit 0.3 mm and current 3 mA.

Interaction of halloysite nanotubes with porphyrine

Two samples of halloysites (H3 and H11) were finally selected for the interaction with TMPyP [5, 10, 15, 20 - tetrakis (1-methyl-4-pyndyl) - 21H, 23H-porphyrine, tetra-p-tosylate salt]. The samples were homogenized in an agate mortar and 1 g of each was then added to the solution of porphyrine TMPyP prepared by mixing of 0.1037 g of porphyrine with 76 ml of distilled water. These mixtures interacted 7 days. After this time the mixtures were centrifuged and the supernatant was poured off. The centrifuged samples leaved to dry and then they were measured by powder X-ray diffraction (pXRD) and diffuse reflectance spectroscopy (DRS).

Table 1. List of halloysite and kaolinite samples and their mineralogical composition obtained by pXRD.

Sample	Source deposit	Mineral phases
H1	Biela hora, Michalovce, Slovakia	halloysite 7 Å, kaolinite, quartz
H2	Matauri Bay, New Zealand	halloysite 7 Å, kaolinite, quartz, cristobalite
H3	Zunyi, China	halloysite 10 Å
H4	Dragon Mine, Utah, USA	halloysite 10 Å, kaolinite, alunite
H5	Qianxi, China	halloysite 10 Å
H6	Dafang, China	halloysite 10 Å, quartz
H7	Turplu, Balikesir, Turkey	halloysite 10 Å, kaolinite, quartz, alunite, gibbsite
H8	Ba Ye Dong Dafang, China	halloysite 10 Å
H9	Ba Ye Dong Dafang, China	halloysite 10 Å
H10	Ilicaiboba, Balikesir, Turkey	halloysite 10 Å, kaolinite, gibbsite, quartz, illite
H11	Turplu, Balikesir, Turkey	halloysite 10 Å
H12	commercial sample	halloysite 7 Å, kaolinite, cristobalite, alunite
KGa-1b	Washington County, Georgia, USA	kaolinite
KGa-2	Warren County, Georgia, USA	kaolinite

ANALYTICAL METHODS

Mineralogical composition of bulk and OP samples as well as their intercalates with formamide and porphyrine were determined by pXRD using the PANalytical X´PertPRO diffractometer with Co-Kα radiation (40 kV and 30 mA) and X'Celerator detector.

The measured diffraction patterns were examined by the HighScorePlus 2.2.5. software, PANanalytical b.v., Almelo, NL. The database JCPDS PDF2, Sets 1-54, International Centre for Diffraction Data, Newtown, Pennsylvania, U.S.A., 2004, was used for the phase identification. The clay minerals were interpreted according to Moore and Reynolds [28].

The bulk samples were measured in the range 4 - 100° 2θ with a step 0.0167° and time of counting 1050 seconds per step. The measuring range of oriented samples (OP) was 4 - 40° 2θ with a step 0.0167 and time of counting 100 seconds per step.

High temperature X-ray diffraction (HT-XRD) was used to study the dehydration of halloysites. All the measurements were carried out on the PANalytical X´PertPRO diffractometer equipped with high temperature chamber Anton Paar HTK-16 which enables heating up to 1200°C. In our dehydration experiments the initial temperature was 25°C and final 120°C with a step of increasing 5°C.

Fourier transform infrared spectroscopy (FT-IR) was used for better distinguishing of low admixtures of kaolinite in natural mixtures. The spectra were recorded in transmission mode, in the 400 - 4000 cm^{-1} range, with a 4 cm^{-1} resolution, using a Thermo Nicolet Nexus 670 FTIR spectrometer with a detector DTGS KBr and a beamsplitter KBr. They were obtained from KBr pressed pellets. These pellets were prepared by homogenous mixing of 1.5 - 4 mg of sample with 300 mg of KBr.

On the samples intercalated with porphyrine, the diffuse reflectance spectra (DRS) were determined by Lambda 35 UV/VIS spectrometer from the company Perkin Elmer with using 50 nm of Ulbricht sphere. Samples were homogenized before in an agate mortar and placed into the silica flask (thickness 2 mm). The range of measured area was from 200 nm to 1100 nm with the step 0.5 nm. The spectra were measured relatively to the standard $BaSO_4$. The absolute $BaSO_4$ reflectance in the area of 350 - 1756 nm is 99 % and more [30]. The measured reflectance was corrected along Kubelk and Munk [31] into the values which are directly proportional to the concentration of the chromophore in the sample. The spectra were processed in the software OriginPro 7.0.

In each sample the content of major oxides (SiO_2, Al_2O_3, Fe_2O_3, TiO_2, CaO, MgO, Na_2O, K_2O and SO_3) was also determined; by gravimetry (SiO_2 and SO_3), chelometric titration (Al_2O_3, CaO and MgO), photometry (Fe_2O_3 and TiO_2), and atomic adsorption spectrometry (Na_2O and K_2O), respectively. The atomic absorption spectrometry (AAS) was also used for the chemical analysis of experimental solutions as described in the chapter "Cation exchange capacity (CEC)".

Description of morphological parameters of halloysite nanotubes was performed by high resolution transmission electron microscopy (HRTEM), with a JEOL TEM 3010 microscope (operating at 300 kV) and equipped with dispersive X-ray analyses facilities. The samples were dispersed in distilled water and sedimented on carbon-coated Cu-microgrids in laboratory conditions.

RESULTS AND DISCUSSION

Mineralogical composition

The list of mineral phases identified in halloysite samples is given in Table 1. The XRD data showed that all samples contain halloysite; while the halloysites H1, H2 and H12 are dehydrated (7 Å), in the remaining samples the hydrated form (10 Å) appears. Kaolinite, quartz, cristobalite, alunite and gibbsite were identified in admixtures (Table 1). The comparison of almost pure halloysite (H11) with sample containing numerous admixtures (H12) is given in Figure 1.

The sample H10 contains K-mica (probably illite) in admixture. Because the most characteristic basal 001 diffraction of illite is overlapped by basal 001 diffraction of halloysite 10 Å, the only way to its positive identification was the previous dehydration of halloysite (Figure 2).

Table 2. Results of chemical analysis (wt. %).

	H2	H3	H4	H5	H6	H7	H8	H9	H10	H11	H12
annealing loss	16.19	27.11	19.23	21.79	24.79	20.56	26.86	23.63	29.01	24.83	21.89
SiO_2	47.4	37.52	43.02	41.44	40.54	41.68	37.34	40.18	30.1	38.96	36.9
Al_2O_3	35.12	34.66	36.39	35.17	33.34	36.12	34.66	35.15	38.74	34.75	37.22
Fe_2O_3	0.37	0.27	0.54	0.18	0.21	0.51	0.26	0.2	0.53	0.38	0.68
TiO_2	0.09	0.02	0.03	0.02	0.02	0.12	0.02	0.04	0.1	0.03	0.09
CaO	< 0.05	< 0.05	< 0.05	< 0.05	< 0.05	< 0.05	< 0.05	< 0.05	< 0.05	< 0.05	0.48
MgO	< 0.05	< 0.05	< 0.05	< 0.05	< 0.05	< 0.05	< 0.05	< 0.05	< 0.05	< 0.05	< 0.05
Na_2O	0.08	< 0.05	< 0.05	< 0.05	< 0.05	< 0.05	< 0.05	< 0.05	0.05	< 0.05	0.32
K_2O	< 0.05	< 0.05	< 0.05	< 0.05	< 0.05	0.13	< 0.05	< 0.05	0.09	< 0.05	1.07
SO_3	0.21	0.16	0.36	0.73	0.15	0.23	0.22	0.21	0.51	0.54	0.64

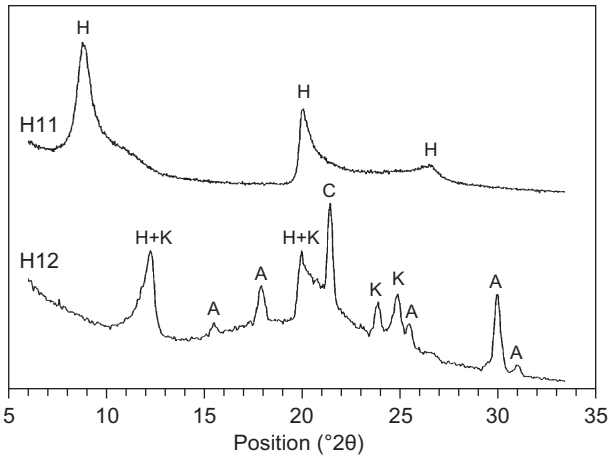

Figure 1. X-ray diffraction patterns of bulk samples of pure halloysite (H11) and halloysite with numerous admixtures (H12); H- halloysite, K- kaolinite, A- alunite, C- cristobalite.

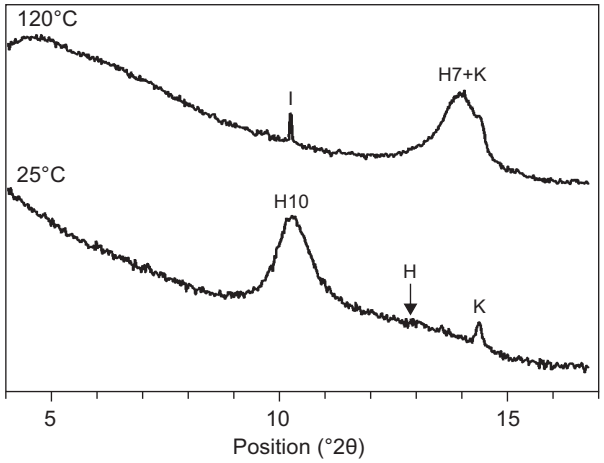

Figure 2. Halloysite H10 before (bottom curve) and after its dehydration (upper curve); on the upper curve, the basal 001 diffraction of K-mica is clearly visible; I - K-mica (probably illite), K - kao-linite, H7 - halloysite 7 Å, H10 - halloysite 10 Å, H - partially dehydrated halloysite.

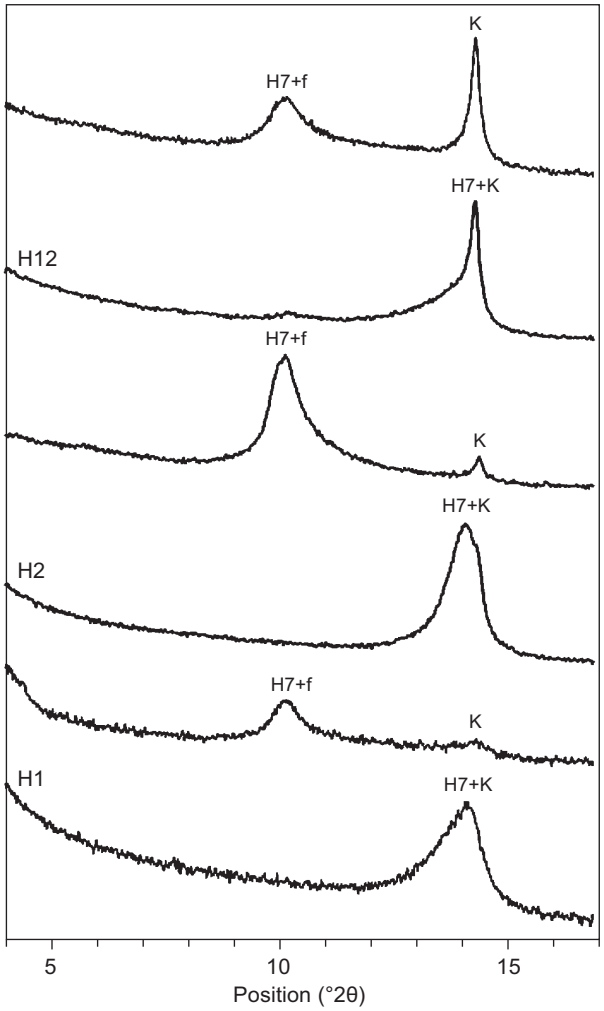

Figure 3. X-ray diffraction patterns of three halloysites 7 Å - the comparison of oriented non-intercalated samples (bottom curves) and the samples intercalated with formamide (upper curves); H7 - halloysite 7 Å, K- kaolinite, H7-f - halloysite 7 Å intercalated with formamide.

While hydrated halloysites 10 Å are relatively pure with only minute admixtures of quartz, the dehydrated halloysites 7 Å contain a significant amount of admixtures. The admixture of kaolinite is difficult to distinguish in a mixture with dehydrated halloysites 7 Å because the basal 001 diffractions of both these minerals overlap each other. This problem can be solved by the interaction of dehydrated halloysite 7 Å with formamide [3, 5, 32, 33]. During this interaction organoclay complex is formed and the 001 diffraction line shifts to the position of 10.2 Å. In the Figure 3 the X-ray patterns of three samples of dehydrated halloysites (H1, H2, and H12) interacted with formamide are shown. While the 001 diffraction of intercalated halloysite is shifted to the position of 10.2 Å, a residual diffraction line at 7 Å confirms the presence of kaolinite (Figure 3).

According to Churchman et al. [3] it is possible to quantify the relative halloysite/kaolinite ratio in the mixture using equation I_{10}/I_7+I_{10}, where I_7 and I_{10} are the intensities of diffractions at 7 Å and 10 Å, respectively. When considering theoretically that contents of halloysite and kaolinite give 100 % thus in our samples their relative ratios are as follows: H1 - 80 % of halloysite and 20 % of kaolinite, H2 - 86 % of halloysite and 14 % of kaolinite, and H12 - 24 % of halloysite and 76 % of kaolinite. The majority of kaolinite in the sample H12 is surprising, because the commercial producer has indicated this sample as halloysite.

The other method to distinguish halloysite and kaolinite in their mixtures is infrared spectroscopy. Halloysite is structurally very similar to kaolinite, but in the infrared spectra it is possible to find some differences. Therefore we compared spectra of halloysites with those of kaolinites (KGa-1b and KGa-2). The main differences are visible at 3600 cm^{-1} and 938 cm^{-1}. The band at 3600 cm^{-1} characterizes the vibration of the interlayer

water and can be recognized only in samples of hydrated halloysites; dehydrated halloysites and kaolinites have no vibration at this position. We found that the samples with the highest content of interlayer water are H3, H5 and H7. The band at 938 cm^{-1} characterizes the vibration of outer hydroxyl groups and it belongs only to kaolinite. Its intensity can therefore be used as a measure of a relative content of kaolinite in the sample. The most intense lines we therefore have in spectra of reference kaolinites, while in spectra of hydrated halloysites are almost invisible (not shown) – it indicates no or only very low admixtures of kaolinite in these samples. These findings almost perfectly confirm the results obtained by pXRD.

Results of chemical analyses are summarized in Table 2. The increased values of K_2O correspond to the content of alunite (H7 and H12) or illite (H10). The explanation of the origin of SO_3 is not fully clear; in samples H4, H7 and H12 it corresponds most probably to alunite and in other samples it could be a part of an amorphous phase, which is not identified by pXRD. The content of iron is relatively very small and variable.

Dehydration of halloysites

The dehydration process of halloysites is described in the literature as spontaneous, fast and irreversible and is promoted by decreasing humidity and/or increasing temperature [5, 6, 34]. To simulate the process, we have measured our samples of hydrated halloysites by HT-XRD under the conditions of decreased relative humidity (20 %) and gradually increasing temperature in the range from 25 to 120°C. A decreased humidity cased an immediate dehydration of halloysites H5, H8 and H10 at 30°C, the other samples dehydrated afterwards when temperature has increased to 35°C (H9), 40°C (H3), 45°C (H6) and 50°C (H11), respectively (Figure 4). The differences in the dehydration temperatures are not significant, the most stable is halloysite H11.

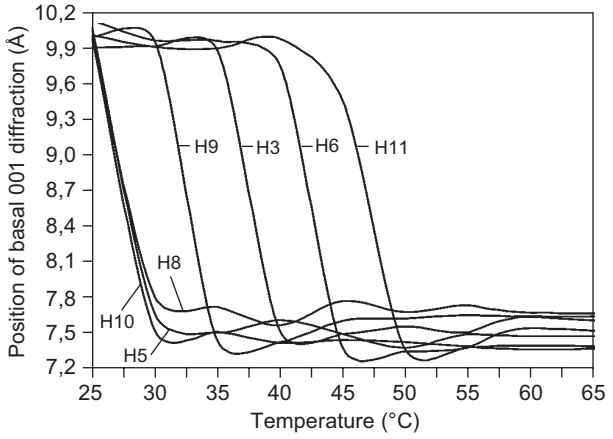

Figure 4. Positions of basal 001 diffractions of pure hydrated halloysites during their heating in the range from 25 to 120°C (in temperatures of 65°C and higher the curves are almost linear).

Morphology of halloysite nanotubes

Within this research we have compared morphological parameters of halloysites on HRTEM images. We have found that tubular shape of particles is prevailing (Figure 5) even in samples where kaolinite is the major admixture. Images were processed manually; an average lengths and widths were calculated from at least ten measurements of individual particles. Average lengths vary between 300 - 1000 nm and their widths between 30 - 100 nm.

Cation exchange capacity (CEC)

The results of the determination of CEC are presented in Table 3. The higher values of CEC correspond to the increased negative charge on particles which is variable in the case halloysites and caused solely by structural defects. The permanent charge is almost 0 similarly to kaolinites. The highest CEC has the sample H10 (7.91 meq/100 g) but this value is affected by numerous admixtures (kaolinite, gibbsite, illite). Among pure hydrated halloysites the highest value of CEC has the sample H11 followed by the sample H3 (Table 3). These samples could thus be potentially the most suitable for the interactions with porphyrine.

Table 3. Cation exchange capacity (CEC) of halloysite samples; samples H3, H5, H9 and H11 are pure hydrated halloysites.

sample	CEC (meq/100 g)
H3	6.5406
H5	5.5542
H9	6.2404
H11	6.7712
H1	7.4935
H2	4.0381
H4	4.1210
H6	5.8422
H7	7.2762
H8	4.6010
H10	7.9088

Interaction of halloysite nanotubes with porphyrine

The samples H11 and H3 have been selected for to be reacted with porphyrine because of their purity (Table 1), optimal morphology and the increased CEC (Table 3).

In the structure of porphyrine N^+ substituted pyrroles are oriented perpendicular to the plane of porphyrine (Figure 6). If the molecules of this porphyrine are adsorbed on the outer surface of clay mineral, the N^+ - pyrrole will turn 90 degrees and thus become parallel to the plane of porphyrine [27] - it causes the colour change of clay mineral and also the spectral change measured by DRS. This specific colour change can be used as indicator that the porphyrine does not intercalate the interlayer space.

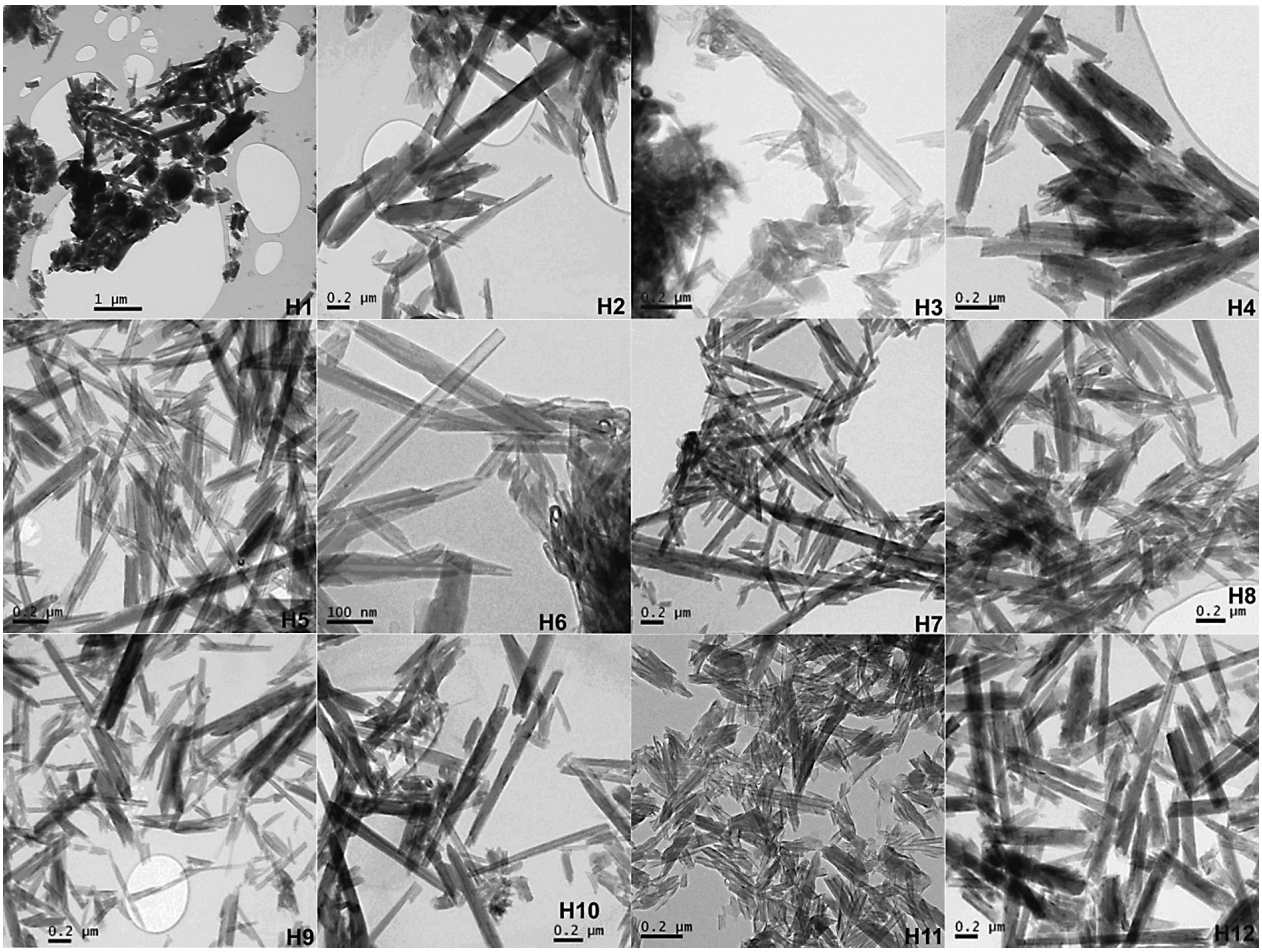

Figure 5. HRTEM images of halloysite samples.

The colour of both of samples (H3, H11) has changed from white to green after their interaction with porphyrine and therefore the sorption took place on the outer surface of halloysite. The proof that the porphyrine does not intercalate into the interlayer of halloysite was done by pXRD. No shift of the basal 001 diffraction towards the lower angles indicating the increasing of interlayer distance was observed. On the contrary, the diffraction line was shifted to higher angles because of halloysite dehydration during the measurement (Figure 7).

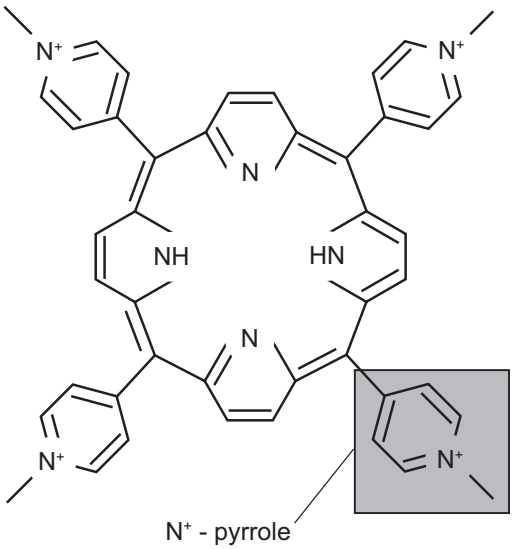

Figure 6. Structure of porphyrine TMPyP; substituted pyrrole N+ oriented perpendicular to the plane of porphyrine.

When interpreting the results of DRS it is possible to find other independent proofs of adsorption processes on the mineral surface during the interaction with porphyrine. This spectrum includes two types of bands: one Soret band and four Q-bands. The Soret band occurs on 420 nm and has important diagnostic significance. The Q-bands occur in between 514 - 640 nm. The spectral change caused by the interaction of porphyrine with halloysite is demonstrated by a specific shifting of Soret band [35, 36].

On the Figure 8 the UV-Vis spectra of interacted samples are compared with that of pure porphyrine. It is clearly visible that the Soret band in both cases has shifted to the value about 470 nm which again indicates that porphyrine is adsorbed on outer surface of halloysite. The intercalation of this type of molecule to the interlayer space has thus been definitely excluded. The areal distribution of porphyrine molecules on the outer surface of halloysite that includes both interior and exterior of the tubes remained unclear.

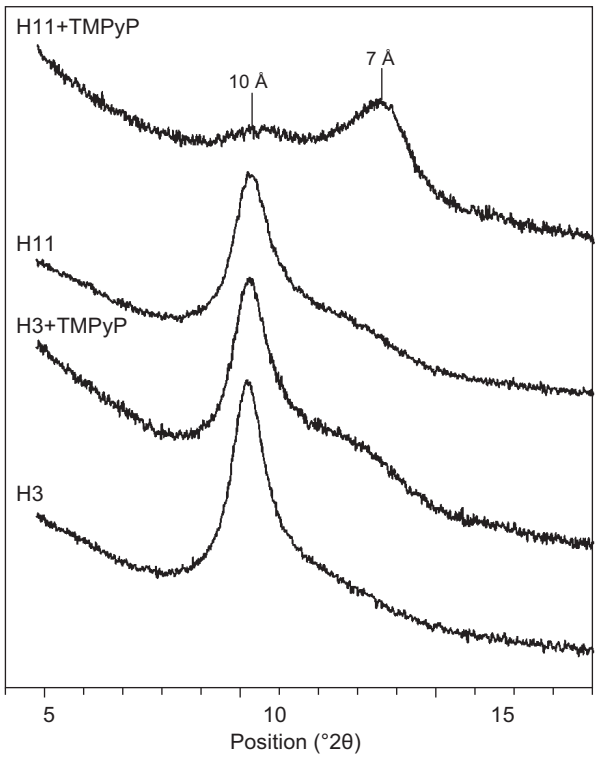

Figure 7. X-ray diffraction patterns of two samples of halloysites without porphyrine (H3, H11) and after their interaction with porphyrine (H3+TMPyP, H11+TMPyP); 10 Å - diffraction of hydrated halloysite; 7 Å - diffraction of dehydrated halloysite.

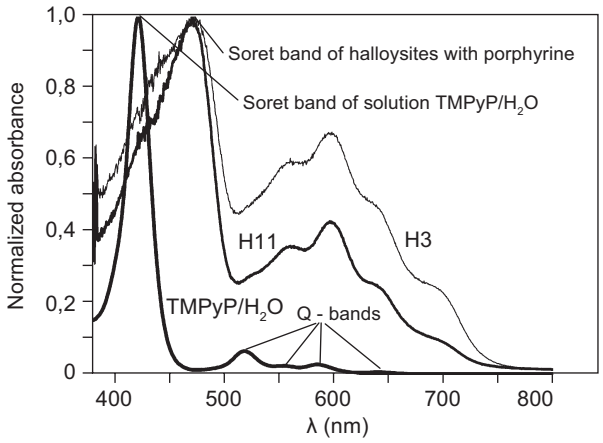

Figure 8. UV-vis spectra of porphyrine in the aqueous solution (TMPyP+H2O) and after its adsorption on two samples of halloysites (H3, H11).

CONCLUSIONS

From the total number of twelve investigated samples of halloysites were eleven of them natural (taken from their deposits) and one of them commercial (supplied by Sigma-Aldrich). In three samples the dehydrated form of halloysite (7 Å) was prevailing and in nine other samples the hydrated form of halloysite (10 Å) predominated. The admixtures of kaolinite and quartz appeared very frequently; the content of kaolinite predominated in the commercial sample. Hydrated halloysites with the highest purity came from three different deposits in China (samples H3, H5 and H8-9) and also from Turplu in Turkey (H11). The hydrated form dehydrates easily and irreversibly in temperatures up to 50°C. The morphology of all samples of halloysites was tubular, but the lengths and diameters of tubes varied significantly. Two samples of very pure tubular halloysites with the highest values of CEC (obtained by optimised AgTU method) - H11 (Turplu, Turkey) and H3 (Zunyi, China) - have finally been chosen for the interactions with porphyrine. Both of them behave similarly during the experiment. We found that porphyrine do not intercalate the interlayer space of halloysite (in the contrast to e.g. formamide), but it is adsorbed on the surface of the clay particles. The production of singlet oxygen is achieved regardless the actual spatial distribution of porphyrine molecules on the clay surface and therefore also this type of interaction is suitable for these specific purposes.

Acknowledgement

Financial support by RVO 61388980 is kindly acknowledged. The authors also thank their colleagues Mariana Klementová for providing HRTEM measurements, and Silvie Švarcová for her help with CEC determinations.

REFERENCES

1. Weiss Z., Kužvart M.: *Jílové minerály: jejich nanostruktura a využití*, p.69, Karolinum, Praha 2005.
2. Kohyama N., Fukushima K., Fukami A.: Clay Clay Miner. *26*, 25 (1978).
3. Churchman G.J., Whitton J.S., Claridge G.G.C., Theng B.K.G.: Clay Clay Miner. *32*, 241 (1984).
4. Giese R.F. in: *Hydrous Phyllosilicates (exclusive of micas)*, p.29-66, Ed. Bailey S.W., Reviews in Mineralogy *19*, Chelsea 1988.
5. Joussein E., Petit S., Churchman J., Theng B., Righi D., Delvaux B.: Clay Miner. *40*, 383 (2005).
6. Kautz C.Q., Ryan P.C.: Clay Clay Miner. *51*, 252 (2003).
7. Bailey S.W. in: *Surface Chemistry Structure and Mixed Layering of Clays*, p.89-98, Ed. Farmer V.C, Tardy Y., Sciences Géologiques, Mémoire *86*, Strasbourg 1990.
8. de Souza Santos P., de Souza Santos H., Brindley G.W.: Am. Mineral. *51*, 1640 (1966).
9. Singer A., Zarei M., Lange F.M., Stahr K.: Geoderma *123*, 279 (2004).
10. Churchman G.J., Davy T.J., Aylmore L.A.G., Gilkes R.J., Self P.G.: Clay Miner. *30*, 89 (1995).
11. Hart R.D., Gilkes R.J., Siradz S., Singh B.: Clay Clay Miner. *50*, 198 (2002).
12. Bobos I., Gomes C.: Can. Mineral. *36*, 1615 (1998).
13. Harvey C.C., Murray H.H.: Appl. Clay Sci. *11*, 285 (1997).
14. Lee S.Y., Gilkes R.J.: Geoderma *126*, 59 (2005).
15. Wilson I.R.: Clay Miner. *39*, 1 (2004).

16. Churchman G.J.: Clay Clay Miner. *38*, 591 (1990).
17. Churchman G.J., Theng B.K.G.: Clay Miner. *19*, 161 (1984).
18. Frost R.L., Kristóf J.: Clay Clay Miner. *45*, 551 (1997).
19. Frost R.L., Kristóf J., Paroz G.N., Kloprogge J.T.: J. Colloid. Interf. Sci. *208*, 216 (1998a).
20. Frost R.L., Kristóf J., Horvath E., Kloprogge J.T.: Spectrochim. Acta *A 56*, 1191 (2000a).
21. Kristóf J., Frost R.L., Kloprogge J.T., Horvath E., Gabor M.: J. Therm. Anal. Calorim. *56*, 885 (1999).
22. Theng B.K.G., Churchman G.J., Whitton J.S., Claridge G.G.C.: Clay Clay Miner. *32*, 249 (1984).
23. Jin H.G., Jung S.Y., Kwon O.Y., Lee J.M.: Industrial report, Korea Research Institute of Chemical Technology, South Korea (2003).
24. Gallagher L.A., Marinho F.J., Jeffcoate C.S., Gershun A.: Application: U.S., 11 (2004).
25. Kasseh A., Chaouki J., Ennajimi E.: U.S. Patent Application, WO2004063259, USA (2004).
26. Shirai J., Inai I., Wakabayashi H., Osuka K., Kato M., Usuki A.: U.S. Patent Application, 703927, USA (2004).
27. Čeklovský A., Czímerová A., Lang K., Bujdák J.: Pure Appl. Chem. *81*, 1385 (2009).
28. Moore, D., Reynolds R.C. (Jr.): 2nd ed.: Oxford University Press, New York (1997).
29. Dohrmann R.: Appl. Clay Sci. *34*, 38 (2006).
30. Weidner V.R., Hsia J.J.: *J. Opt. Sos. Amer*. *71*, 856 (1981).
31. Sherman D.M.: Phys. Chem. Miner. *12*, 161 (1985).
32. Frost R.L., Kristóf J., Horvath E., Kloprogge J.T.: Langmuir *17*, 3216 (2001b).
33. Joussein E., Petit S., Delvaux B.: Clay Miner. *35*, 17 (2007).
34. Churchman G.J.: PhD thesis, University of Otago, New Zealand (1970).
35. Chernia Z., Gill D.: Langmuir *15*, 1625 (1999).
36. Tagaki S., Shimada T., Eguchi M., Yui T., Yoshida H., Tryk D.A., Inoue H.: Langmuir *18*, 2265 (2002).